Arch. Metall. Mater. **64** (2019), 2, 727-732

DOI: 10.24425/amm.2019.127605

W. MAZIARZ*, A. WOJCIK*#, R. CHULIST*, M.J. SZCZERBA*, M. KOWALCZYK**,
P. CZAJA*, E. CESARI***, J. DUTKIEWICZ*

THE EVOLUTION OF MICROSTRUCTURE AND MAGNETO-STRUCTURAL PROPERTIES OF HEAT TREATED Ni-Mn-Sn-In HEUSLER ALLOYS SINTERED BY VACUUM HOT PRESSING

In this work, vacuum hot pressed Ni-Mn-Sn-In Heusler alloys with different concentration of In (0, 2 and 4 at.%), were investigated. The magneto-structural behaviour and microstructure dependencies on chemical composition and on heat treatment were examined. It was found that the martensite start transformation temperature increases with growing In content and to a lesser extent with increasing temperature of heat treatment. The high energy X-ray synchrotron radiation results, demonstrated that both chemical composition as well as temperature of heat treatment slightly modified the crystal structures of the studied alloys. Microstructural investigation performed by transmission electron microscopy confirmed chemical composition and crystal structure changes in the alloys.

Keywords: Ni-Mn-Sn Metamagnetic Shape Memory Alloys; Sintering Process; Heat Treatment; Electron Microscopy

1. Introduction

Ni-Mn-Z (Z = Sn, In) Heusler alloys are interesting from scientific and application points of view. Their unique properties, such as an inverse magnetocaloric effect, elastocaloric effect and metamagnetic shape memory effect, are associated with martensitic transformation. The transformation occurs between the high temperature, high symmetry phase – austenite with ferromagnetic ordering and low temperature, low symmetry martensite showing weak magnetic (antiferro- and/or paramagnetic) behaviour [1-4]. It is generally known that the temperature range of martensitic transformation and multifunctional properties of Ni-Mn-based Heusler alloys are strongly dependent on (*i*) chemical composition [5] and (*ii*) fabrication methods, which influence the microstructural features of materials [6,7].

Among several fabrication methods, including conventional casting or rapid crystallization process (e.g. melt-spinning), powder metallurgy drives interest due to geometrical advantages of the product (increased efficiency in magnetic refrigeration) and due to the economic factor (low-cost fabrication method of materials in powder form or dense following sintering). Moreover, it is worth to mention that powder metallurgy is a very effective technique for limiting the intrinsic brittleness of the Ni-Mn-based Heusler alloys [8,9].

Here, we have investigated the influence of both chemical composition as well as heat treatment on martensitic transformation temperatures, crystal structure and microstructure of Ni-Mn-Sn-In metamagnetic shape memory alloys sintered by vacuum hot pressing method.

2. Experimental

The alloys with nominal composition of $Ni_{50}Mn_{37.5}Sn_{12.5-x}In_x$ (x = 0, 2, 4 at.%), hereafter referred as In0, In2 and In4, were fabricated by vacuum hot pressing of powders, previously manufactured by milling of melt-spun ribbons. The sintering process was performed at 920 K for 30 min under uniaxial applied pressure of 320 MPa [10]. Subsequently, sintered samples were cut into smaller pieces and heat treated at 873 K, 973 K and 1073 K for 2 hours, what was followed by quenching in ice water. Structure of alloys at room temperature was determined by high-energy synchrotron X-ray radiation measurements (DESY, Hamburg). To establish a good grain statistics and to eliminate texture effect, the samples were continuously rotated 180° around the ω-axis [11,12]. That allowed collecting diffraction patterns from all grains enclosed in the measured volume. As a next, the measured 2D pattern were integrated using the Fit2D software. Microstructure and chemical composition were examined by Philips XL30 Scanning Electron Microscope (SEM) and Tecnai G2 Transmission Electron Microscope (TEM) equipped with an energy dispersive X-ray microanalyser (EDX). Samples for

* INSTITUTE OF METALLURGY AND MATERIALS SCIENCE, POLISH ACADEMY OF SCIENCES, 25 REYMONTA STR., 30-059 CRACOW, POLAND
** WARSAW UNIVERSITY OF TECHNOLOGY, FACULTY OF MATERIALS SCIENCE AND ENGINEERING, 141 WOLOSKA STR., 02-507 WARSAW, POLAND
*** UNIVERSITAT DE LES ILLES BALEARS, DEPARTAMENT DE FÍSICA, PALMA DE MALLORCA, SPAIN
# Corresponding author: a.wojcik@imim.pl,

SEM observations were prepared by manual polishing followed by electropolishing using an electrolyte of perchloric acid (20%) and ethanol (80%). Thin foil samples for TEM observations were prepared with TenuPol-5 double jet electropolisher using an electrolyte of nitric acid (1/3) and methanol (2/3) at temperature of about 243 K. Martensitic transformation behaviours were investigated by differential scanning calorimetry using Mettler DSC 823 instrument with cooling/heating rate of 10 K min^{-1}. Magnetic measurements were performed using Physical Properties Materials System PPMS with VSM mode.

3. Results and discussion

Figure 1 shows a set of SEM micrographs of the sintered alloys with different compositions (In0, In2, In4) after heat treatment under various conditions (873 K, 973 K, 1073 K). It can be seen that vacuum hot pressing leads to formation of dense microstructure, despite the fact that boundaries between particles remain clearly visible. The average grain size in the heat-treated, sintered alloys is smaller than the particles size and it was estimated in the range of 10-12 µm. It is, thus, much smaller than in conventionally fabricated alloys (arc melting, induction melting), where grain size is in the range of hundreds of µm [13]. Moreover, it can be concluded that both temperature of heat treatment as well as In concentration had no influence on the average grain size of sintered alloys. Additionally, it can be noted that the porosity level in alloys containing 4 at.% of In is much higher than for alloys with lower In concentration. In the case of the In0 and In2 only a small amounts of fine pores were observed. It was found in the case of as-sintered materials and described in previous work [10]. This phenomenon can be connected with hardness of the powders.

In our previous work, we have reported that as-sintered samples were chemically inhomogeneous. Large second-phase regions, enriched in Ni and Mn were found [10]. Figure 2 presents

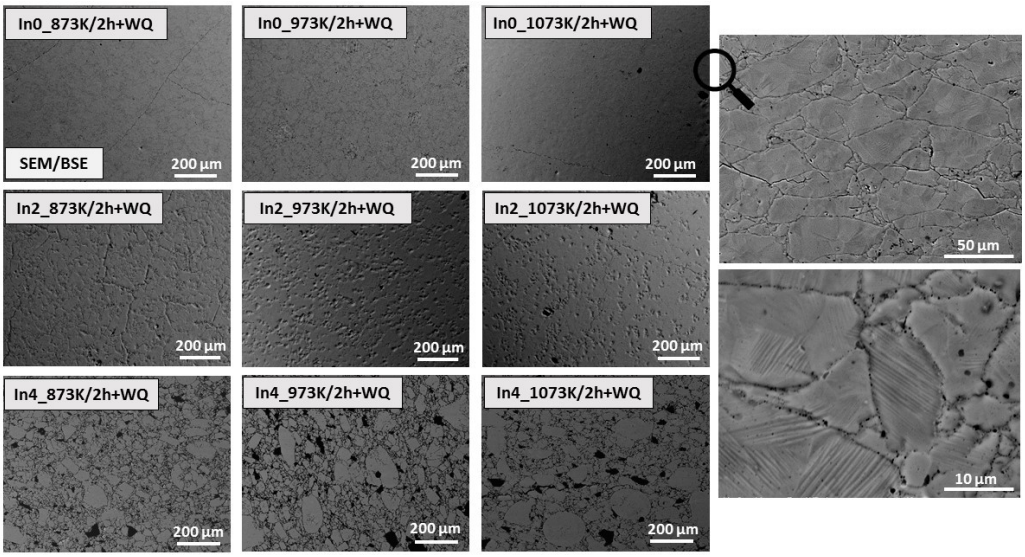

Fig. 1. Set of SEM images for In0, In2 and In 4 heat treated at different temperatures

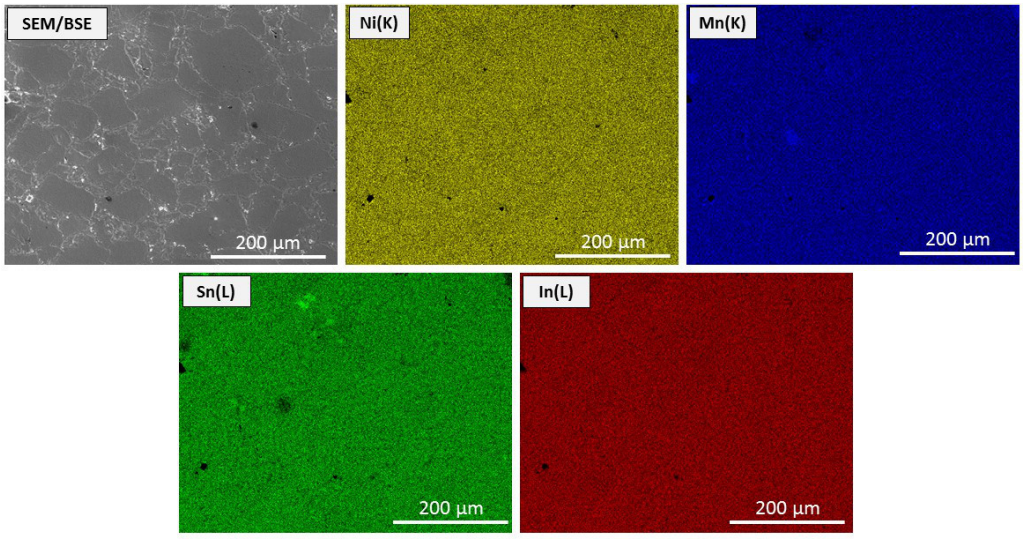

Fig. 2. SEM image and corresponding EDS mapping analysis for In2_973K/2h+WQ

SEM image with corresponding elemental energy dispersive spectroscopy (EDS) maps for Ni, Mn, Sn and In, respectively, taken from the polished surface of the In2_973K/2h+WQ sample. The EDS maps clearly show that the alloy after heat treatment is chemically homogeneous. Moreover, no signs of additional phases were detected.

Figure 3 illustrates room temperature high energy synchrotron diffraction patterns of In0, In2 and In4 alloys heat treated at different temperatures (873 K, 973 K, 1073 K). High energy synchrotron radiation measurements are more advantageous than conventional X-ray sources because the *peak*-to-*background ratio* is higher, and the signal is obtained from a larger volume of material. Hence, the investigation of two-phase materials are more precise. As-sintered In0 alloy exhibits the two-phase structure consisting of the $L2_1$ austenite and martensite identified as four-layered structure with monoclinic distortion (4M) [10]. Samples annealed at 873 and 973 K contain a mixture of the $L2_1$ austenite and 4M martensite, while the alloy annealed at 1073 K, gives peaks, which can be indexed based on the five-layered (5M) martensite. The In2 alloy, regardless of the temperature of heat treatment, contains a mixture of the cubic $L2_1$ austenite, and 4M and 5M martensites (both monoclinic). Similar situation has been found for samples containing 4 at.% of indium. What is interesting, the crystal structure of both as-sintered as well as heat treated samples maintains the same. Thus, it can be concluded that the crystal structure of all investigated alloys does not significantly rest on the concentration of In as well as on the temperature of heat treatment.

The detailed microstructural investigation has been performed by TEM. Figures 4(a-c) present exemplary bright field (BF) images of In2 after annealing at 873 K showing martensite plates within the grains. Corresponding selected area diffraction patterns (SADP) presented in Figure 4(d) can be well indexed in accordance with the four-layered (4M) martensite along the $[0\bar{1}2]$ zone axis. One can see three satellite spots between two fundamental maxima, which is a typical feature of diffraction patterns for the four-layered structure. A high-resolution TEM image (HRTEM) is presented in Figure 4(e) showing the modulated martensitic structure. Small inset shows fast Fourier transform (FFT) from the area marked by the red square confirming four-layered structure of martensite. Furthermore, inverse fast Fourier transform (IFFT) is presented in Figure 4(f). Martensite phase has periodic stacking of planes with the $(2\bar{2})$ sequence according to Zhdanov notation.

Figure 5 represents differential scanning calorimetry (DSC) curves for In0, In2 and In4 heat treated at 873, 973 and 1073 K, respectively. Upon cooling, large exothermic peaks correspond to forward martensitic transformation from austenite to martensitic phase (A→M). During heating, reverse martensitic transformation takes place (M→A). The characteristic martensite start (finish) transformation temperatures M_s (M_f), and the reverse martensitic transformation temperatures A_s (A_f) were estimated by the two-tangent method. The thermal hysteresis of the transformation (ΔT) was estimated as $\Delta T = A_f - M_s$. The obtained results are listed in Table 1. To confirm estimated values of temperatures of structural transformation magnetic

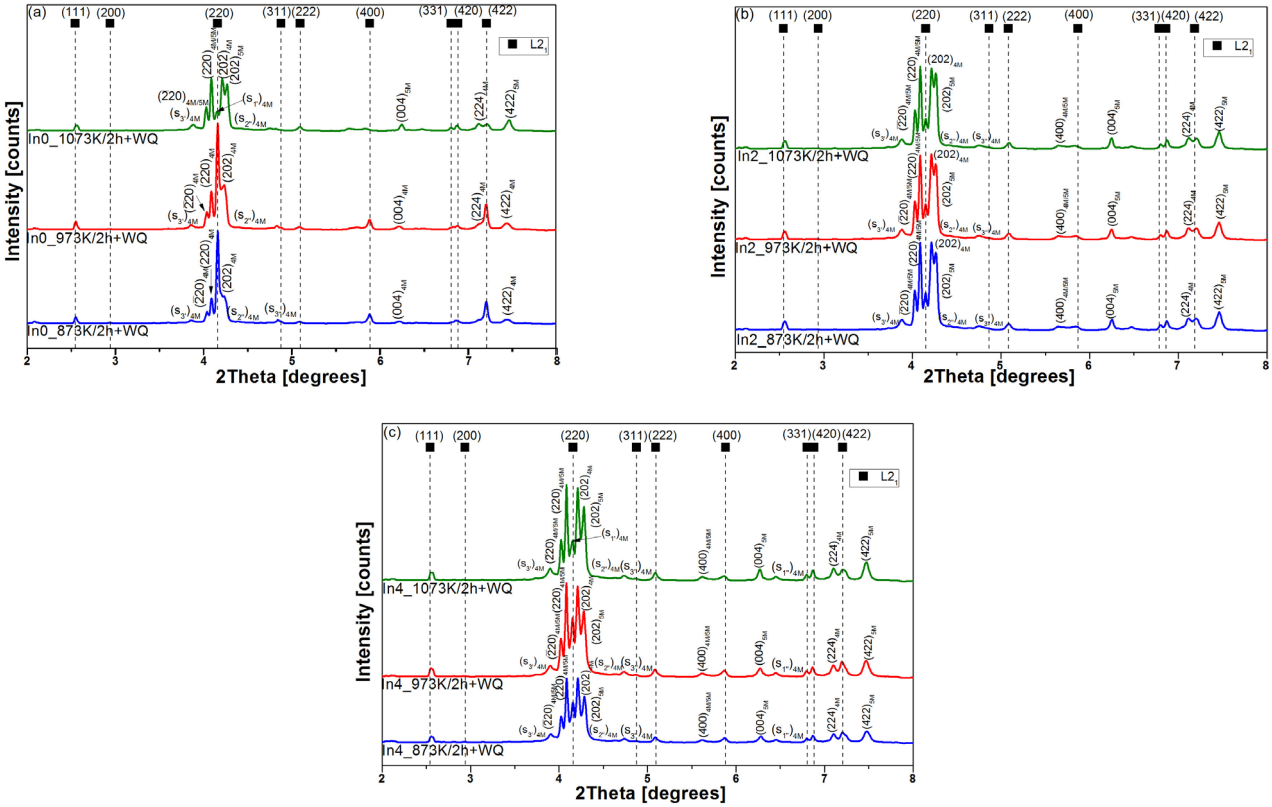

Fig. 3. The high energy synchrotron diffraction patterns of In0 (a), In2 (b) and In4 (c) specimens after heat treatment, recorded at room temperature

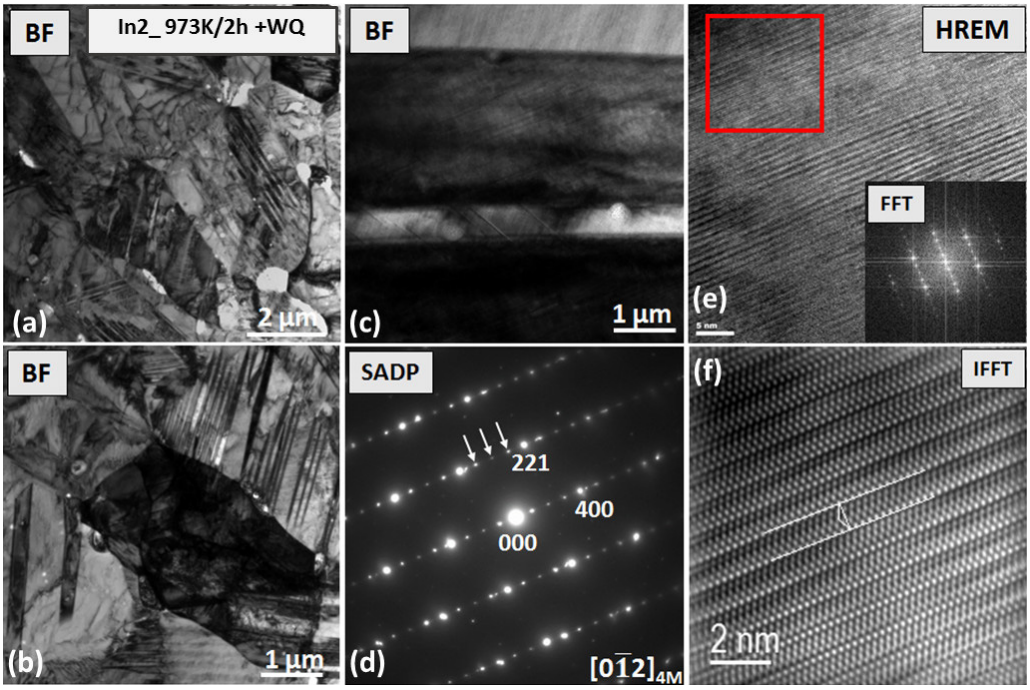

Fig. 4. Bright fields images (a), (b) and (c); corresponding selected area diffraction patterns (d); high resolution electron microscopy image (e) and corresponding inverse Fourier transform (f). Smaller inset shows fast Fourier transform from the red square visible in HREM image

measurements have been carried out. Figure 6(a-c) represents field-cooling and field-heating curves under low magnetic field of 100 Oe for all investigated specimens. The results obtained by magnetic measurements are comparable and in good agreement with the DSC results. For In0 (Fig. 6(a)) upon cooling, an increase of magnetization due to magnetic transition of austenite at Curie temperature (T_c^A) is visible, while both martensitic transformation and magnetic transition are very close each other. With further cooling, large increase of magnetization is related to magnetic transition of martensite (T_c^M). The In2 and In4 show slightly different behaviour, which derives from the closer proximity between the M_s and T_C^A, and entails larger paramagnetic

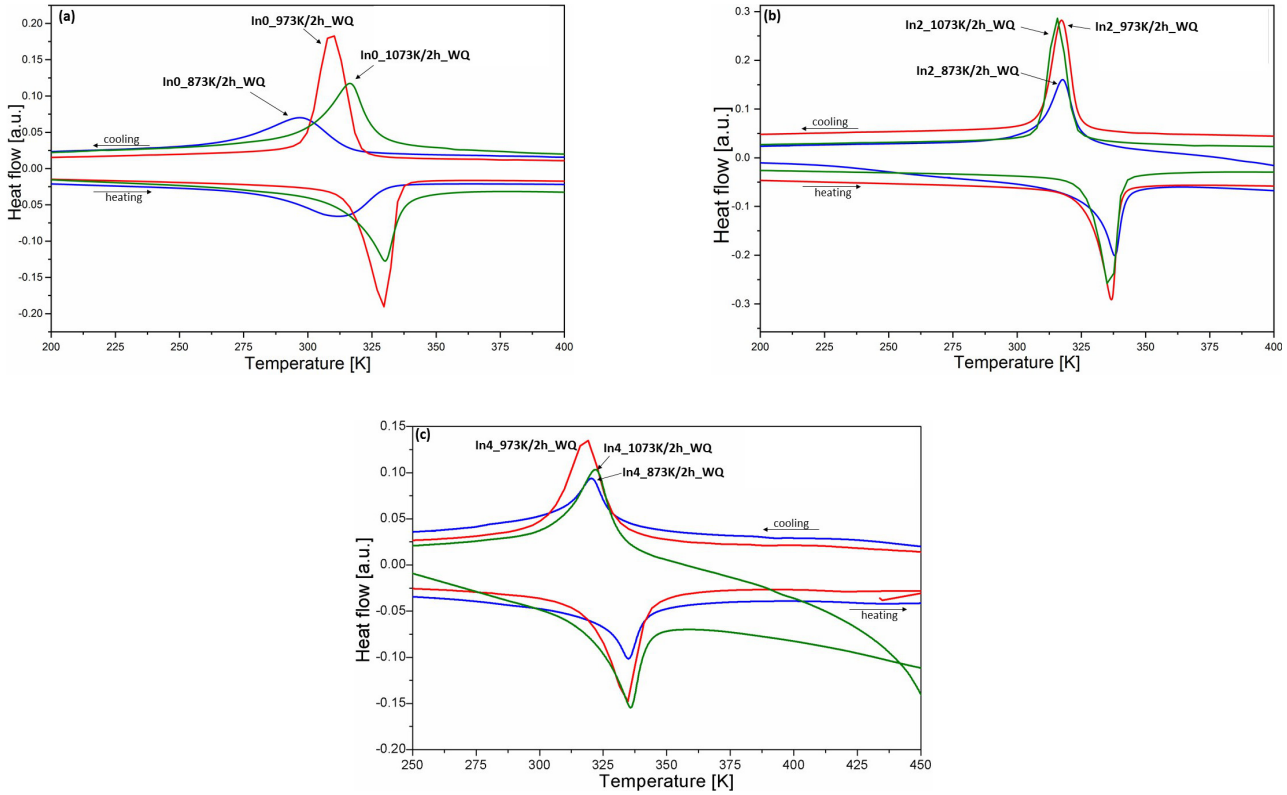

Fig. 5. DSC curves for In0 (a), In2 (b) and In4 (c)

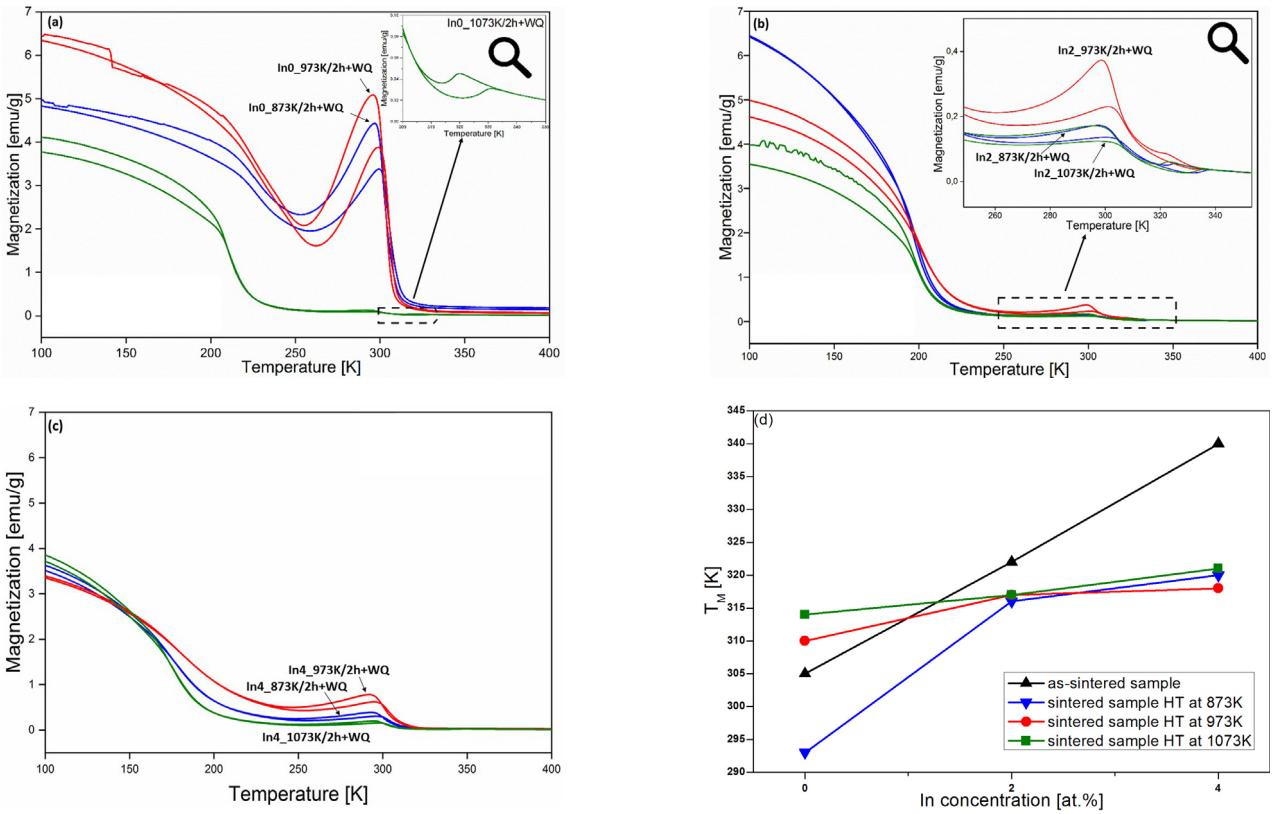

Fig. 6. Magnetization versus temperature curves at low magnetic field of 100 Oe for In0 (a), In2 (b) and In4 (c); (d) Martensitic transformation temperature (T_M),calculated from (M_s + M_f)/2 vs. Indium concentration

fraction of austenite taking part in the transformation. Moreover, one can see that for In0 and In2, two-step martensitic transformation occurs. The same effect was observed for powders and as-sintered alloys with the same chemical composition [10,14].

TABLE 1

Characteristic temperatures of martensitic and reverse martensitic transformation temperatures for sintered In0, In2 and In4 alloys after heat treatment

Alloy	Temperature (K)				
	M_s	M_f	A_s	A_f	ΔT
In0_873K/2h+WQ	318	267	283	332	14
In0_973K/2h+WQ	320	300	315	336	16
In0_1073K/2h+WQ	328	300	318	339	11
In2_873K/2h+WQ	323	308	326	342	19
In2_973K/2h+WQ	324	309	327	341	17
In2_1073K/2h+WQ	325	309	327	343	18
In4_873K/2h+WQ	328	312	326	342	16
In4_973K/2h+WQ	329	306	312	345	16
In4_1073K/2h+WQ	333	309	318	344	11

Overall, we have examined the effect of both the chemical composition and the heat treatment at various temperatures on magneto-structural behaviour of sintered Ni-Mn-Sn-In alloys. It is well-known that the martensitic transformation temperature in Ni-Mn-Sn based Heusler alloys is very sensitive to chemical composition modified either by (i) stoichiometry [15] and/or (ii) the addition of other elements such as Fe, Cu, Co etc. [16-18]. In the presented case, it can be noticed that temperatures of martensitic transformation increase with indium concentration (Fig. 6(d)). This behaviour is against both well-established (i) electron to atom (e/a) ratio and (ii) unit-cell volume influences on the martensitic transformation [5]. Thus, another factors such as atom ordering or even change in the hybridization states between the 3d orbitals of Mn and Ni should be taken into account [19]. Hence, the effect of In substitution and heat treatment may result from the complex interplay between the atomic ordering and microstructural evolution as a consequence of relaxation of internal stresses introduced during sintering process.

4. Conclusions

The sintered bulk alloys with the nominal compositions $Ni_{50}Mn_{37.5}Sn_{12.5}In_x$ (x = 0, 2, 4 at.%) were obtained by vacuum hot pressing from powders produced by vibration milling of melt-spun ribbons. The sintered alloys were then heat treated at various temperatures what was followed by water quenching. It was found that both chemical composition (indium concentration) as well as heat treatment temperature have an effect on martensitic transformation temperatures and crystal structure of sintered Ni-Mn-Sn-In alloys. The results show that powder metallurgy combined with subsequent heat treatment can be interesting for development of functional Ni-Mn based shape memory alloys.

Acknowledgement

This work has been carried out within the statutory activity of IMMS PAS (Z-10).

REFERENCES

[1] T. Krenke, E. Duman, M. Acet, E.F. Wassermann, X. Moya, L. Manosa, A. Planes, Nature **4**, 450 (2005).

[2] R. Kainuma, K. Oikawa, W. Ito, Y. Sutou, T. Kanomata, K. Ishida, J. Mater. Chem. **18**, 1837 (2008).

[3] H. Zheng, W. Wang, S. Xue, Q. Zhai, J. Frenzel, Z. Luo, Acta Mater. **61**, 4648 (2013).

[4] P.O. Castillo-Villa, L. Manosa, A. Planes, D. Soto-Parra, J.L. Sanchez-Llamazares, H. Flores-Zuniga, C. Frontera, J. Appl. Phys. **113**, 053406 (2013).

[5] V.A. Chernenko, Scripta Mater. **40**, 523 (1999).

[6] Y. Zhang, Q. Zheng, W. Xia, J. Zhang, J. Du, A. Yan, Scripta Mater. **104**, 41 (2015).

[7] A. Wójcik, W. Maziarz, M.J. Szczerba, M. Kowalczyk, E. Cesari, J. Dutkiewicz, Intermetallics **100**, 88 (2018).

[8] X.H. Tian, J.H. Sui, X. Zhang, X. Feng, W. Cai, J. Alloys Compd. **509**, 4081 (2011).

[9] X.H. Tian, J.H. Sui, X. Zhang, X.H. Zheng, W. Cai, J. Alloys. Compd. **514**, 210 (2012).

[10] W. Maziarz, A. Wójcik, J. Grzegorek, P. Czaja, M.J. Szczerba, J. Dutkiewicz, A. Żywczak, E. Cesari, J. Alloys. Compd. **715**, 445 (2017).

[11] R. Chulist, L. Straka. A. Sozinov, T. Lippmann, W. Skrotzki, Scripta Mater. **68**, 671 (2013).

[12] E. Pagounis, R. Chulist, T. Lippmann, M. Laufenberg, W. Skrotzki, Appl. Phys. Lett. **103**, 111911 (2013).

[13] B. Tian, D. Ren, Y. Tong, F. Chen, L. Li, Y. Zheng, Mater. Sci. Forum **815**, 222 (2015).

[14] W. Maziarz, A. Wójcik, P. Czaja, A. Żywczak, J. Dutkiewicz, Ł. Hawełek, E. Cesari, J. Magn. Magn. Mater. **412**, 123 (2016).

[15] W. Maziarz, P. Czaja, M.J. Szczerba, L. Lityńska-Dobrzyńska, T. Czeppe, J. Dutkiewicz, J. Alloys Compd. **615**, 173 (2014).

[16] C.O. Aguilar-Ortiz, D. Soto-Parra, P. Alvarez-Alonso, P. Lazpita, D. Salaraz, P.O. Castillo-Villa, H. Flores-Zuniga, V.A. Chernenko, Acta Mater. **107**, 9 (2016).

[17] H.C. Xuan, P.D. Han, D.H. Wang, Y.W. Du, Intermetallics **54**, 120 (2014).

[18] A. Gosh, K. Mandal, Eur. Phys. J. B **86**, 378 (2013).

[19] M. Khan, J. Jung, S.S. Stoyko, A. Mar, A. Quetz, T. Samanta, I. Dubenko, N. Ali, S. Stadler, K.H. Chow, Appl. Phys. Lett. **100**, 172403 (2012).